

## Cross-shelf transport of warm and saline water in response to sea ice drift on the Laptev Sea shelf

Markus A. Janout,<sup>1</sup> Jens Hölemann,<sup>1</sup> and Thomas Krumpfen<sup>1</sup>

Received 2 November 2011; revised 5 October 2012; accepted 28 October 2012; published 4 February 2013.

[1] Oceanographic moorings and conductivity-temperature-depth (CTD) surveys from September 2009 to September 2010 are used to describe recent changes in the Laptev Sea hydrography and to highlight wind- and ice-driven surface Ekman transport as the mechanism to translate these changes from the outer- to the inner-shelf bottom waters. In February 2010, moored oceanographic instruments recorded a sudden increase in temperature (+0.8°C) and salinity (+ >3) near the bottom of the inner Laptev Sea shelf. Such warm and saline waters had not been previously observed on the inner shelf in winter. They likely originated from the basin and were first observed during a summer 2009 CTD survey in the northwestern shelf break region, subsequently spreading east and shoreward across the Laptev Sea shelf. The changes were introduced to the mooring site by the first of a series of bottom-intensified flow events with velocities reaching 20 cm s<sup>-1</sup>, topographically guided along a relic submarine river valley. Each of the flow events coincided with negative pressure anomalies at the mooring site and offshore-directed (upwelling-favorable) winds and ice drift. We suggest that the observations to first order resemble a simplified two-dimensional two-layered ocean, where offshore surface Ekman transport is compensated for by a barotropic shoreward response flow near the bottom. In this paper, we use one of the first comprehensive long-term Laptev Sea datasets to highlight ice-ocean-atmosphere interactions in early and late winter and discuss the role of freshwater, stratification, and ice mobility on under-ice circulation on the Laptev Sea shelf.

**Citation:** Janout, M. A., J. Hölemann, and T. Krumpfen (2013), Cross-shelf transport of warm and saline water in response to sea ice drift on the Laptev Sea shelf, *J. Geophys. Res. Oceans*, 118, 563–576, doi:10.1029/2011JC007731.

### 1. Introduction

[2] Heat and salt entering the Arctic Ocean through Fram Strait and the Barents Sea from the Atlantic is transported cyclonically along the continental margins in a boundary current [Aagaard, 1989; Rudels *et al.*, 1999a; Woodgate *et al.*, 2001]. The Arctic Ocean's upper layer and the pack ice cover are separated from the warm Atlantic waters by a strong halocline, which is replenished with shelf-modified waters along the continental slopes [Aagaard *et al.*, 1981]. As the boundary current propagates along the Eurasian continental slope, it loses heat and salt due to lateral mixing of different branches [Rudels, 2012], mixing by slope convection [Ivanov and Golovin, 2007], double diffusion [Rudels *et al.*, 1999b], or turbulent vertical mixing [Lenn *et al.*, 2009]. However, the turbulent fluxes measured in the boundary current near the Lomonosov Ridge poleward of the northeastern Laptev Sea are nearly one order of magnitude too low to close the heat budget, which suggests that

heat may be lost laterally [Lenn *et al.*, 2009], although specifics remain unknown. Previous surveys reported the occurrence of warm and saline waters above the steep Laptev Sea shelf break and outer-shelf regions [Schauer *et al.*, 1997; Rudels *et al.*, 2000], although the impact of these waters on oceanic and sea ice conditions on the shelf remains unclear due to a lack of observations.

[3] The wide and shallow Laptev Sea shelf features strong polynya activity along the extensive landfast ice edge (Figure 1) and exports large amounts of sea ice [Alexandrov *et al.*, 2000] and riverine freshwater [Guay *et al.*, 2001] into the Transpolar Drift and the Arctic basin. While ocean-to-atmosphere transfer of upwelled heat may be favored in coastal polynyas of narrow shelves such as the Beaufort Sea [Pickart *et al.*, 2009], the central Laptev Sea polynyas are far removed from the shelf break and the influence of upwelled Atlantic-derived waters. In addition, the inner Laptev Sea shelf, i.e., the shallower southern region near the Lena Delta, is strongly impacted by the Lena River runoff, and stratification further complicates mixing in near-shore polynyas. As opposed to those in the northwestern Laptev Sea, southern Laptev Sea polynyas do not form waters dense enough [Winsor and Björk, 2000; Krumpfen *et al.*, 2011] to ventilate and maintain the arctic halocline [Aagaard *et al.*, 1981]. While recent studies focused on mixing processes on the Laptev Sea slope [Lenn *et al.*, 2011; Polyakov *et al.*, 2012] and sea-ice formation in inner-shelf polynyas [Dethleff

<sup>1</sup>Alfred Wegener Institute for Polar and Marine Research, Bremerhaven, Germany.

Corresponding author: M. A. Janout, Alfred Wegener Institute for Polar and Marine Research, Am Handelshafen 12, D-27570 Bremerhaven, Germany. (Markus.Janout@awi.de)

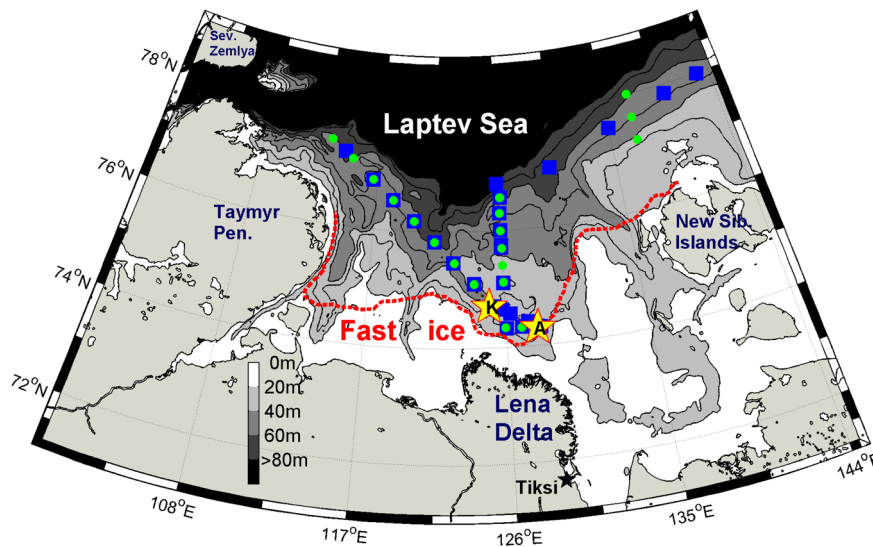


**Figure 1.** Map of the Laptev Sea, including International Bathymetric Chart of the Arctic Ocean (IBCAO) [Jakobsson *et al.*, 2008] bathymetry contours, Khatanga (KH) and Anabar (AN) mooring locations (yellow stars, K and A), and September 2009 (blue squares) and September 2010 (green circles) CTD stations. The red dashed line defines the March 2010 boundary between landfast ice (inshore) and pack ice (offshore), based on ENVISAT images. Polynyas are frequent seaward of the fast ice edge throughout the Laptev Sea [Bareiss and Gørgen, 2005].

*et al.*, 1998; Willmes *et al.*, 2011], little is known about the under-ice circulation on the vast central shelf, the transition zone between fresh coastal waters, and the warm and saline shelf break waters.

[4] Dmitrenko *et al.* [2010] speculated on the role of Atlantic-derived waters on the outer shelf, and described intrusions of warmer (+0.2°C) and more saline (+1.0–1.5) waters to inner-shelf polynya regions. However, solar radiation may increasingly warm waters during extended summer open water periods [Perovich *et al.*, 2008], and hence positive temperature anomalies exist and may remain in the sea ice season, trapped in the interior water column by salinity stratification [Hölemann *et al.*, 2011]. Therefore, temperature anomalies, thermohaline gradients, and the role of Atlantic-derived water masses on this shelf are neither sufficiently documented nor understood. Nevertheless, Dmitrenko *et al.* [2010] further discussed intrusions that may occur along relic submarine river valleys following upwelling-favorable winds and, although based on incomplete datasets, provided some indications for wind-driven under-ice transport. This complemented earlier modeling studies by Harms *et al.* [2003], which showed near-bottom salinity intrusions in the Kara Sea, evidently in response to offshore wind events.

[5] With this paper, we aim to continue the discussion on transport processes that take place under the ice of the vast central Laptev Sea shelf, in the transition zone between the fast ice edge, and the steep continental shelf break. We use one of the few existing long-term Laptev Sea mooring records to highlight the occurrence of anomalously warm and saline waters, which arrived on the inner shelf with the first in a series of bottom-intensified flow events. These bottom flows occurred along a submarine river valley in response to surface Ekman transport during enhanced offshore wind and ice drift events and can be viewed as one piece in the insufficiently understood puzzle of the Laptev Sea winter circulation.

[6] The paper is organized as follows. After introducing the data and methods in section 2, we present results in section 3 on sea ice (section 3.1) and oceanic (section 3.2) conditions and investigate the origin and fate of the inflow (section 3.3) as well as its forcing mechanism (section 3.4). A summary is given in section 4 before the discussion and conclusions (section 5).

## 2. Data, Methods, and Setting

[7] Two oceanographic moorings, “Khatanga” (KH, 74.7°N, 125.3°E, water depth 43 m) and “Anabar” (AN, 74.3°N, 128.0°E, water depth 33 m) (Figure 1), were deployed in September 2009 during Transdrift 16 (RV *Yakov Smirnitsky*) and recovered in September 2010 during Transdrift 17 (RV *Nikolay Evgenov*) as part of the Russian-German “Laptev Sea System” project. Both moorings were located at the offshore end of the West New Siberian and the Anabar/Lena polynyas [Zakharov, 1966; Bareiss and Gørgen, 2005]. The location of AN was near the landfast ice edge and hence directly affected by polynya processes, as opposed to KH, which was located ~50–70 km away from the fast ice edge.

[8] The moorings were equipped with two Teledyne-RDI Workhorse Sentinel Acoustic Doppler Current Profilers (ADCP), one upward looking 300 kHz ADCP moored ~3 m above the bottom and one downward looking 1200 kHz instrument moored ~6 m above bottom. Velocity profiles were averaged in 30 min ensembles with a bin size of 1 m (0.2 m) for the 300 kHz (1200 kHz) instrument with 67 (110) pings per ensemble. Velocity data with beam correlation of <64% or an error of >3 cm s<sup>-1</sup> were discarded, and the standard deviation after the quality screening was 1.6 cm s<sup>-1</sup> (2.2 cm s<sup>-1</sup>) for the 300 kHz (1200 kHz) ADCP at both KH and AN. Compass accuracy is ±2°, and calibration was carried out before each deployment. The magnetic declination in the region is -17°,

and none of the four ADCPs showed compass problems. The first bin of the 300 kHz (1200 kHz) ADCP was located 3.18 m above (0.7 m below) the transducer head at  $\sim 7$  m ( $\sim 5.2$  m) above bottom. The bottom track velocities of KH's 300 kHz ADCP were used as ice drift velocities. The bottom track depth measures the distance from the transducer to the underside of the sea ice from October to May and was used to estimate relative ice thickness. The bottom track uses one burst of pings per ensemble. When ice is absent, return signals are faulty, error velocities rise rapidly, and the measurement is rejected. The compass was additionally verified by comparing ADCP-measured ice drift with remotely sensed ice drift velocity and direction during strong polynya events. The accuracy of the bottom track depth was estimated at 15 cm, based on a comparison with the mooring's pressure data. For more details on these methods, refer to *Shcherbina et al.* [2005] and *Hyatt et al.* [2008].

[9] One RBR XR-420 CTTu measuring conductivity and temperature was mounted on each ADCP frame. The quality of the temperature data is good (accuracy  $0.002^\circ\text{C}$ ), while the unpumped conductivity sensor showed a strong drift due to bio-fouling after a few months of deployment. One Seabird MicroCAT (SBE37) conductivity-temperature-depth (CTD) was mounted  $\sim 5$  m above bottom. The accuracies for temperature and conductivity are  $0.002^\circ\text{C}$  and  $0.0003 \text{ S m}^{-1}$ , respectively. The moorings were designed to remain within  $\sim 10$  m of the bottom for sufficient clearance from drifting pressure ridges. KH was situated in one of the numerous  $\sim 50$  km wide relic submarine river valleys found on the Laptev Sea shelf, featuring depressions  $< 10$  m deeper than the surrounding waters. The internal Rossby Radius of Deformation  $R = NH/f$ , where  $N$  is stratification,  $H$  a vertical length scale, and  $f$  the Coriolis force, varies depending on the Lena River plume and stratification but is always smaller ( $5\text{--}8$  km) than the width of these valleys, which suggests that ageostrophic processes related to abruptly changing topography should not be expected. In contrast to wide and deep arctic canyons such as Barrow Canyon [*Weingartner et al.*, 1998] or Mackenzie Trough [*Williams et al.*, 2006], the shallow submarine Laptev Sea depressions may favor cross-shelf transport between the inner and central shelves but do not contribute to shelf-basin exchange.

[10] CTD data obtained during Transdrift 16 and 17 (Figure 1) were collected with a Seabird SEACAT profiler (SBE19), which provides initial accuracies for temperature and conductivity of  $0.005^\circ\text{C}$  and  $0.0005 \text{ S m}^{-1}$ , respectively. The Laptev Sea data collection of the Arctic and Antarctic Research Institute (AARI), St. Petersburg was used to put our 2010 observations into a historical context. The AARI dataset consists of  $> 5000$  profiles since 1930 and is described in detail in *Dmitrenko et al.* [2008]. Each profile (January–December) from a depth of  $< 100$  m and from locations east of  $140^\circ\text{E}$  and south of  $78^\circ\text{N}$  with more than two data points was linearly interpolated to 1 m depth bins. Following this preparation, temperature and salinity values from 30, 40, 50, and 60 m were extracted to provide a uniform basis for a comparison with our mooring, which recorded temperature and salinity of approximately  $-0.9^\circ\text{C}$  and  $\sim 33$  in late winter/spring 2010 in a water depth of 38 m. The comparison will be presented in section 3.3.

[11] Monthly sea ice drift information was obtained from the IFREMER webpage (<ftp://ftp.ifremer.fr/ifremer/cersat/>

products/gridded/psi-drift/data/). The merged product is based on Advanced Scatterometer (ASCAT) and Special Sensor Microwave Imager (SSM/I) daily drift data available on a  $62.5 \text{ km} \times 62.5 \text{ km}$  grid [*Ezraty et al.*, 2010]. Consecutive Environmental Satellite (ENVISAT) Synthetic Aperture Radar (SAR) images were used to delineate fast ice positions. The ENVISAT C-band wide swath data is VV-polarized and covers an area of approximately  $400 \times 800 \text{ km}^2$  with a spatial resolution of  $150 \text{ m}^2 \times 150 \text{ m}^2$ .

[12] Wind data was downloaded from the National Centers for Environmental Prediction (NCEP) at <http://www.esrl.noaa.gov>. Open water in polynyas can significantly alter atmospheric conditions in the region on scales smaller than those resolved by NCEP [*Ernsdorf et al.*, 2011]. However, our ADCP's bottom track indicates no apparent open water periods between November 2009 and May 2010 at KH, and therefore we expect that NCEP provides a good representation of the regional wind field. Table 1 provides the summary statistics of KH mooring and wind data.

[13] The energy spectrum on the Laptev Sea shelf is dominated year-round by semidiurnal tidal ( $M_2, S_2$ ) and inertial ( $f$ ) frequencies. While these high frequencies govern smaller scale mixing processes, this paper is focused mainly on the advective property changes which are governed by lower-frequency processes with periods of  $> 2$  days. Therefore, currents, ice drift, and pressure data were low-passed using a seventh order Butterworth filter in order to extract the subtidal frequencies. Our 2009/2010 records provide one of the first complete yearlong Laptev Sea data collections of bottom CTD, ADCP, and local sea ice information and allow a comprehensive look into ice-ocean-atmosphere interactions that govern oceanographic winter processes on this shelf.

### 3. Results

#### 3.1. Ice Conditions in 2009/2010

[14] The local ice drift velocities at KH were derived from the ADCP in bottom track mode, agree well with remotely sensed ice drift data (Figure 2), and are regionally representative of inner Laptev Sea shelf ice conditions [*Rozman et al.*, 2011]. In general, ice motion in the vicinity of the mooring was governed by the prevailing winds, with a predominant eastward drift from November to January with magnitudes of  $10\text{--}20 \text{ cm s}^{-1}$  (Table 1, Figure 2). Then, from February to April, the ice drift changed direction to westward with reduced velocities of  $3\text{--}6 \text{ cm s}^{-1}$ . Relative to January, February–April showed a 1.3 m increase in bottom track-derived ice thickness (Table 1). In May, ice breakup started, and average ice thickness decreased and drift velocities increased to  $> 30 \text{ cm s}^{-1}$ . The magnitude and strength of the ice drift is further controlled by the coastline and the presence of landfast ice. For instance, offshore ice drift or a drift path that is orientated parallel to the fast ice edge shows significantly higher velocities (December and January). In contrast, during onshore drift or ice drift orientated toward the coast of Severnaya Zemlya (Figure 1), the sea ice drift speed is significantly reduced (February and April). The coastline and the presence of landfast ice may reduce ice drift velocities and further immediately impact the under-ice circulation on the Laptev Sea shelf, as will be discussed in the following.

**Table 1.** Monthly Summary Statistics of Ice Drift, Wind, Currents, and Near-bottom Temperature and Salinity at Mooring KH (74.7°N, 125.2°E) from October 2009 to August 2010<sup>a</sup>

	Oct	Nov	Dec	Jan	Feb	Mar	Apr	May	Jun	Jul	Aug
Ice drift (ADCP bottom track)											
Magnitude (cm/s)	26.8 (15.5)	19.6 (14.5)	10.4 (7.7)	11.3 (10.1)	3.4 (4.1)	6.2 (5.6)	4.4 (5.6)	22.8 (17.6)	n/a	n/a	n/a
Direction (deg)	289°	115°	64°	107°	268°	337°	172°	325°	n/a	n/a	n/a
Principal axis and variance explained (%)	134° (64.7)	104° (72.6)	79° (65.3)	104° (54.7)	18° (74.9)	28° (54.3)	8° (75.4)	33° (50.8)	n/a	n/a	n/a
Ice thickness (m) inferred from bottom track depth	0	+0.3	+0.8	+0.9	+2.2	+2.1	+2.3	+0.9	n/a	n/a	n/a
NCEP Wind (75°N, 125°E)											
Speed (m/s)	11.1 (2.6)	14.9 (3.5)	13.0 (2.9)	13.5 (3.1)	11.7 (2.3)	10.5 (2.2)	15.0 (3.2)	11.5 (2.6)	12.3 (3.1)	10.0 (2.4)	18.0 (3.4)
Direction (deg)	316°	113°	90°	90°	214°	346°	138°	269°	262°	61°	45°
Principal axis and variance explained (%)	157° (63.4)	75° (73.7)	62° (65.5)	12° (52.6)	107° (86.0)	100° (65.8)	68° (64.4)	46° (81.6)	115° (71.4)	106° (62.9)	98° (56.4)
SBES37 (38m)											
Mean salinity	31.68 (0.26)	31.88 (0.24)	31.68 (0.25)	30.93 (0.60)	30.24 (1.33)	32.67 (0.30)	33.15 (0.17)	33.10 (0.11)	33.16 (0.20)	33.13 (0.20)	33.05 (0.34)
Min/Max salinity	30.93/32.13	30.93/32.20	30.61/32.08	28.83/31.75	28.75/32.86	31.53/33.28	32.69/33.38	32.33/33.37	32.01/33.46	32.47/33.48	31.43/33.43
Mean temperature (°C)	-1.59 (0.03)	-1.31 (0.25)	-1.08 (0.17)	-1.15 (0.21)	-1.40 (0.28)	-0.88 (0.05)	-0.88 (0.02)	-0.90 (0.02)	-0.96 (0.02)	-1.03 (0.04)	-1.05 (0.06)
Min/Max temperature (°C)	-1.64/-1.47	-1.60/-0.92	-1.44/-0.56	-1.57/-0.55	-1.61/-0.83	-1.17/-0.78	-0.93/-0.81	-1.13/-0.85	-1.15/-0.91	-1.26/-0.98	-1.26/-0.99
ADCP currents											
10–20 m mean											
Current magnitude (cm/s)	14.6 (4.3)	11.6 (3.7)	7.2 (1.7)	7.9 (2.9)	6.4 (1.5)	6.7 (1.3)	7.5 (1.4)	10.0 (4.0)	15.9 (4.0)	13.5 (4.1)	16.6 (5.8)
Max. velocity	50.9	40.1	23.6	36.4	22.1	30.6	30.6	41.5	48.4	67.0	68.1
Residual flow and direction	3.9 (170°)	4.5 (106°)	2.2 (77°)	0.8 (44°)	0.7 (342°)	0.2 (27°)	1.3 (307°)	2.0 (123°)	9.3 (116°)	1.6 (155°)	4.2 (93°)
Principal axis (deg) and variance explained (%)	17° (68.9)	152° (68.0)	136° (78.4)	160° (91.1)	173° (92.2)	160° (79.0)	168° (90.1)	173° (61.5)	4° (82.9)	174° (61.9)	20° (76.3)
20–30 m											
Current magnitude (cm/s)	11.5 (3.7)	8.6 (2.9)	8.0 (1.6)	8.1 (2.7)	6.8 (1.8)	6.4 (1.5)	9.2 (1.8)	9.5 (3.2)	14.5 (3.8)	13.9 (3.8)	14.1 (4.6)
Max. velocity	19.8	17.0	11.3	20.3	10.2	9.0	13.3	15.8	26.6	24.9	29.5
Residual flow and direction	2.8 (150°)	4.0 (102°)	1.5 (65°)	0.8 (31°)	0.8 (347°)	0.3 (184°)	2.2 (319°)	2.7 (177°)	8.6 (133°)	0.8 (211°)	4.0 (94°)
Principal axis (deg) and variance explained (%)	157° (86.3)	2° (73.7)	132° (73.9)	169° (87.9)	1° (89.9)	172° (87.3)	173° (92.2)	169° (66.7)	169° (82.6)	160° (60.0)	175° (72.2)
30–40 m											
Current magnitude (cm/s)	10.6 (4.3)	7.5 (3.2)	7.0 (1.5)	8.4 (2.5)	7.8 (1.6)	9.0 (2.5)	9.1 (1.8)	8.5 (2.8)	9.9 (4.4)	9.0 (2.1)	9.8 (4.0)
Max. velocity	22.6	18.2	11.9	16.6	11.1	14.2	13.6	16.1	23.2	14.6	19.4
Residual flow and direction	1.3 (98°)	2.0 (78°)	1.0 (334°)	1.7 (315°)	0.4 (16°)	2.1 (176°)	1.7 (185°)	3.8 (158°)	3.8 (133°)	0.7 (1°)	2.1 (80°)
Principal axis (deg) and variance explained (%)	124° (93.3)	138° (81.2)	117° (81.0)	165° (85.1)	166° (83.9)	164° (92.6)	159° (88.9)	152° (60.1)	160° (69.7)	118° (80.7)	126° (88.6)

<sup>a</sup>Bold numbers in parentheses after wind speed, temperature and salinity, and current magnitude indicate one standard deviation. The residual current magnitude was computed from the monthly averaged zonal and meridional components. Wind and current direction follow the oceanographic convention (i.e., 90° means flow to the east, 180° flow to the south, etc.). Monthly mean ice thickness estimates were derived from ADCP bottom track depth, and the values are thickness relative to October 2009.  
KH, Khatanga; ADCP, Acoustic Doppler Current Profilers.

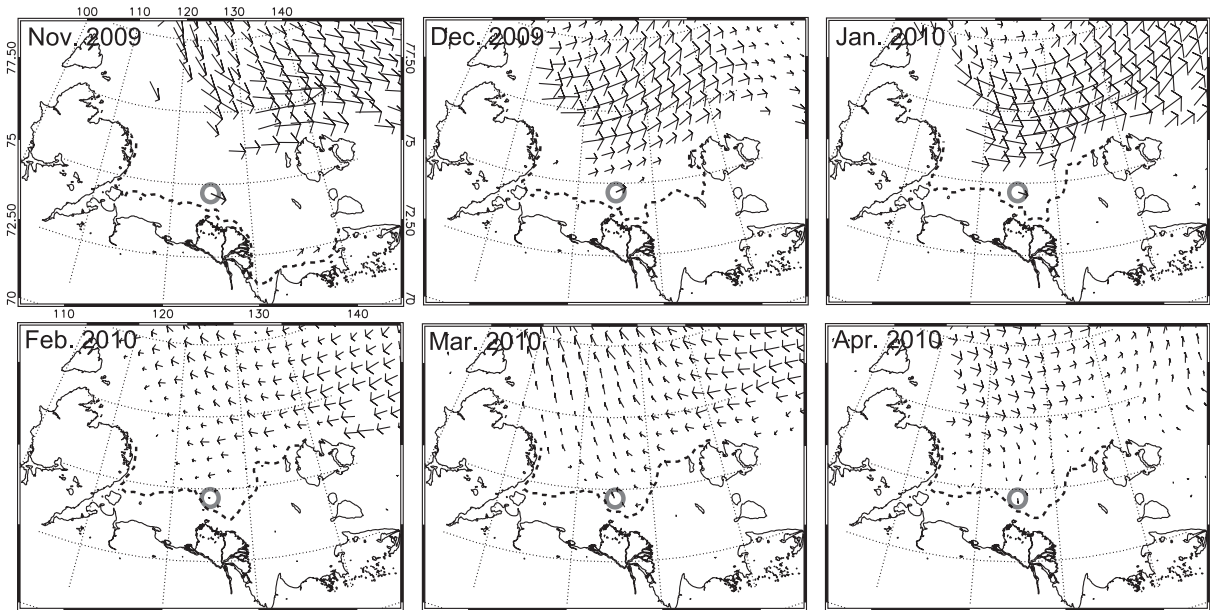


**Figure 2.** Monthly (November 2009 to April 2010) satellite-based sea ice drift in the Laptev Sea (black arrows pointing to the direction of flow). The position of the fast ice edge is indicated by the dashed line. The thick arrow framed by the gray circle shows magnitude and direction of ice drift computed from the Acoustic Doppler Current Profiler (ADCP) in bottom track mode at the mooring KH. Note that monthly ice drift at KH is also shown in Table 1.

### 3.2. One Year of Mooring-based Oceanographic Conditions on the Inner Laptev Sea Shelf in 2009/2010

#### 3.2.1. Fall/Early Winter 2009

[15] The year-round near-bottom temperature and salinity records at KH (Figure 3a) show a high degree of variability and allow insights into the relevant processes taking place on the inner Laptev Sea shelf. In September 2009, before freeze-up, near-bottom temperature and salinity were constant at  $-1.6^{\circ}\text{C}$  and 32, respectively. Vertical velocity shear (i.e., vertical current differences) was maximum in the upper 15–20 m (Figure 3c), coincident with the halocline (pycnocline) depth in September 2009 (Figure 4a). Since no stratification data are available after September 2009, the depth of the maximum vertical shear is used as an estimate for mixed layer depth [van Haren, 2000; Howard et al., 2004]. The first strong wind and polynya event after freezeup occurred on 10 November 2009 (yearday  $-50$  in Figure 3; note that we chose a date convention for our 2009/2010 time series, where noon on 1 January 2010 is day 0.5 and noon on 31 December 2009 is day  $-0.5$ ), and coincided with a sudden advected temperature increase to  $-1.0^{\circ}\text{C}$  and a salinity decrease from 32 to 31 over the course of 5 days. The event introduced a  $\sim 3$  month-long period (yeardays  $-45$  to  $+40$ ) characterized by enhanced wind and sea ice motion (Table 1, Figure 7), temperature variability between  $-1.6^{\circ}\text{C}$  and  $-0.6^{\circ}\text{C}$ , and a gradual salinity decrease from 32 to 29.5 (Figure 3a). During this time, the mixed layer depth increased until the water column was well mixed. Since mid-winter water column information is non-existent for the Laptev Sea between November and February, we lack quantitative stratification measures. However, previous studies estimated that the Lena river freshwater influence on southern Laptev Sea polynyas generally prevents dense water formation and convective mixing of the water column [Dmitrenko et al., 2005; Krumpfen et al., 2011] typical of

polynyas in other Arctic regions far from large freshwater sources, e.g., the northwestern Laptev Sea [Aagaard et al., 1981; Martin and Cavalieri, 1989; Winsor and Björk, 2000; Ivanov and Golovin, 2007; Dethleff, 2010]. This, however, does not preclude several processes interacting to enhance vertical mixing. Here we suggest that the  $\sim 2.5$  salinity decrease relative to mid-November 2009 (yearday  $-45$ ) is the result of vertical freshwater redistribution. The bottom salinity of 29.5 at the end of the “mobile ice period” in January 2010 is close to the mean salinity of 29.7 from the September 2009 CTD profile (Figure 4a), which implies a near-balance of all other salt fluxes. In fact, the average residual near-bottom ( $\sim 33$ – $43$  m) flow between mid-November 2009 and mid-February 2010 (yeardays  $-45$  to  $+45$ ) was  $\sim 1.7\text{ cm s}^{-1}$  from the southeast, and east-to-west salinity gradients of  $0.013\text{ km}^{-1}$ , estimated from September 2009 CTD profiles, suggest that advection reduced the salinity near the seafloor by  $\sim 1.7$  over 90 days. In contrast, a mean southeastward flow of  $\sim 1.3\text{ cm s}^{-1}$  and a salinity gradient of  $\sim 0.006\text{ km}^{-1}$  in the upper layer (0–30 m) suggest an upper layer salinity increase of  $\sim 0.6$ . If these estimates hold, the reversing flow directions have a destabilizing effect on the water column, while the total mean surface to bottom advective salt flux is small. A nearly closed salt budget by advection and mixing implies that surface salt fluxes at the mooring location due to brine rejection are likely small. As an alternative estimate, surface salt fluxes due to ice production may be assessed following Martin and Cavalieri [1989] and Winsor and Björk [2000]:

$$\Delta S = \rho_{\text{ice}} \Delta h (S_{\text{oce}} - S_{\text{ice}}) [H_{\text{oce}} \rho_{\text{oce}}]^{-1} \quad (1)$$

[16] We employed our bottom track-based ice thickness estimate, which measured a mean increase of  $\Delta h = 0.6\text{ m}$  between November and January (Table 1) to estimate the

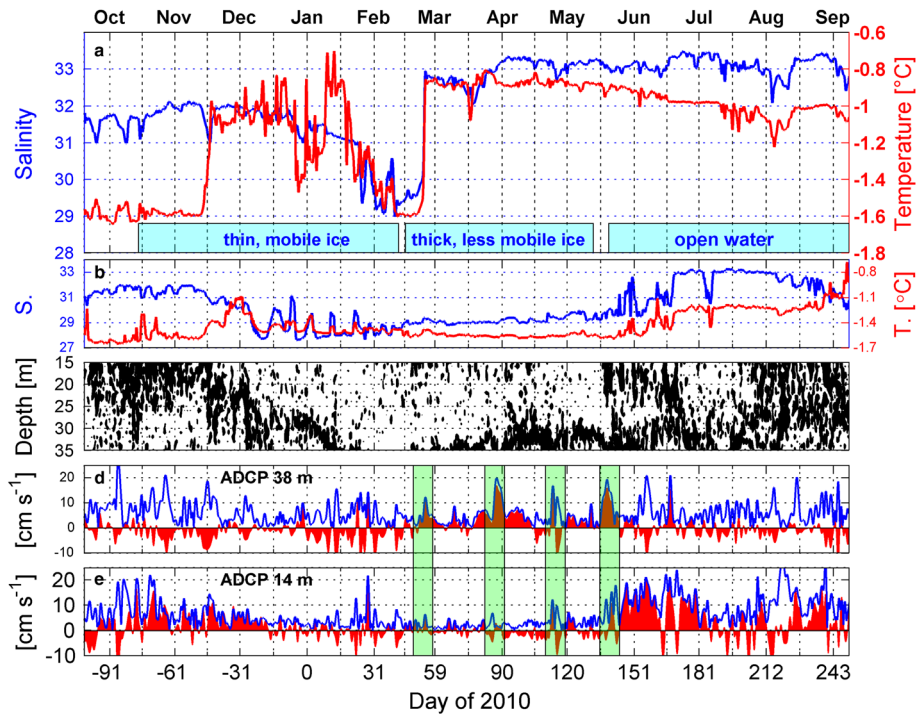


**Figure 3.** Moored near-bottom temperature [ $^{\circ}\text{C}$ ] (red) and salinity (blue) at (a) mooring KH and (b) mooring AN, (c) contours of ( $\geq 0.1$ ) KH shear magnitude [ $\text{s}^{-1}$ ], computed from ADCP data; KH ADCP magnitude [ $\text{cm s}^{-1}$ ] (blue) and down-channel component (red) along the principal axis of variance ( $160^{\circ}$ ) at (d) 38 m and (e) 14 m. Positive velocities indicate onshore flow. Shaded areas in Figures 3d and 3e highlight bottom-intensified flow events. The x axis shows day of the year 2010, with day 0.5 marking noon on 1 January 2010. Each labeled tick marks the beginning of a month. The corresponding months are shown at the top of Figure 3a. The shaded regions in Figure 3a provide a broad reference to the sea ice cover throughout the time series.

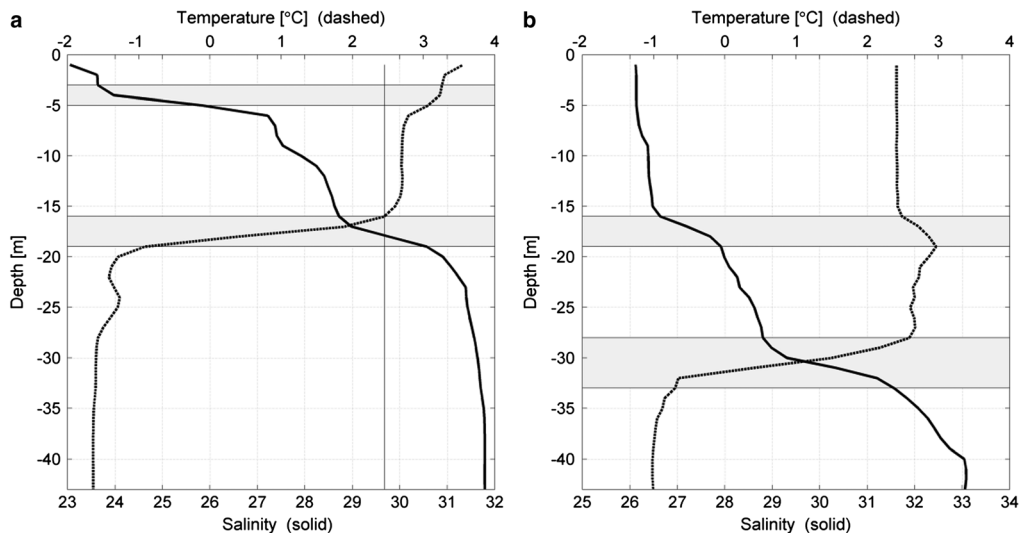


**Figure 4.** Temperature [ $^{\circ}\text{C}$ ] (dashed) and salinity (solid) from (a) September 2009 and (b) September 2010 CTD profiles. Thin line in Figure 4a indicates mean water column salinity. Layers of maximum stratification are shaded.

salt flux [ $\text{kg m}^{-2}$ ], i.e., the numerator in (1), which is further dependent on the sea ice density ( $\rho_{\text{ice}} = 920 \text{ kg m}^{-3}$ ) and the salinity difference between ice ( $S_{\text{ice}}$ ) and water ( $S_{\text{occ}}$ ), and is then divided by the ocean depth ( $H_{\text{occ}} = 43 \text{ m}$ ) and density ( $\rho_{\text{occ}} = 1025 \text{ kg m}^{-3}$ ). Assuming a range of surface salinities

$S_{\text{occ}} = 23\text{--}30$ , based on the September 2009 CTD profile (Figure 4) and the January near-bottom salinity (Figure 3), and an ice salinity of  $S_{\text{ice}} = 0.31(S_{\text{occ}})$  following *Martin and Kauffman* [1981] results in a salinity increase of  $\Delta S = 0.20\text{--}0.26$  during this 2 month period. These estimates are

considerably smaller than those of *Winsor and Björk* [2000] for this region, who considered salinity changes due to ice production over longer periods and in open water areas only. However, since no evidence of open water was found in the ADCP's bottom track data during this time, lower salt fluxes should be expected. These estimates support the above assumption that lateral salt fluxes are more important than surface fluxes, at least in non-polynya regions. This is plausible considering the strong gradients in the vicinity of the Lena freshwater outflow.

[17] The large temperature variability observed in early winter cannot be accounted for by horizontal gradients. Instead, the episodic early winter temperature jumps likely reflect the downward mixing of the internal temperature maximum, i.e., summer-warmed water trapped in the interior water column by salinity stratification, as previously described for the Laptev Sea [Bauch *et al.*, 2009] and the Canada Basin [Jackson *et al.*, 2010].

### 3.2.2. Late Winter/Spring 2010

[18] By early February 2010 (yearday 40), the temperature variability ceased and remained constant at  $-1.6^{\circ}\text{C}$ , while the weak shear levels ( $<0.02\text{ s}^{-1}$ ) now suggest a well-mixed water column. Then, on 22 February 2010 (yearday 52), the temperature (salinity) suddenly increased over the course of 2 days from  $-1.6^{\circ}\text{C}$  to  $-0.9^{\circ}\text{C}$  (29.5 to 33). A close inspection of the three near-bottom temperature records from 3, 5, and 6 m above bottom (40, 38, and 37 m depth) and the ADCP data provides insights into the structure of the inflow (Figure 5). On yearday 52, the temperature sensed closest to the bottom increased from  $-1.4^{\circ}\text{C}$  to  $-0.9^{\circ}\text{C}$  within a few hours (Figure 5a). One day later, the middle temperature increased, and by yearday 54, the temperature was uniform at  $-0.85^{\circ}\text{C}$  at all three levels. The salinity changed accordingly from the bottom upward (not shown). The ADCP data confirm that velocities first increased near the bottom with semidiurnal pulses of  $\sim 10\text{ cm s}^{-1}$  and from yearday 52 with

southeastward velocities peaking at  $\sim 15\text{ cm s}^{-1}$  (Figure 5b). The mooring record also features three additional inflow events in late March, mid-April, and mid-May (around yeardays 86, 111, and 137), all of which occurred near the bottom from the northwest along the principal axis of the submarine river valley with peak velocities reaching  $20\text{ cm s}^{-1}$ .

### 3.2.3. Summer 2010

[19] When temperatures rose above freezing in early May 2010, polynyas immediately evolved into large open water regions. The decrease in ice concentration caused the ice drift velocity to increase and thickness to decrease (Table 1). The currents were then maximum at the surface, characteristic for a wind-driven open water current regime. The average flow direction was southeastward, and strong near-bottom flow events were absent, as opposed to on-average weak upper water column and amplified near-bottom currents under the ice in early and late winter (Figure 3, Table 1). Near-bottom temperature and salinity remained variable and overall higher than at the beginning of the deployment in September 2009. In contrast to 2009, the September 2010 water column showed, besides the seasonal pycnocline at 15 m, a second pycnocline around 30 m induced by the saline near-bottom waters (Figure 4b). This is also reflected in the velocity shear, which was maximum near the bottom after the inflow in February and again in the surface with the beginning of the open water season.

### 3.3. Origin and Fate of the Warm and Saline Waters

[20] Our observations indicate that the warm and saline water mass first measured at KH in February 2010 originated from the northwestern Laptev Sea shelf, where similar properties ( $\sim -1.0^{\circ}\text{C}$ ,  $>33$ ) were found in lower layer ( $>25\text{ m}$ ) waters during a September 2009 CTD survey (Figure 6). While the inner-shelf stations show typical near-freezing bottom temperatures and moderate ( $<32.5$ ) salinities, subpycnocline temperatures (salinities) gradually increase along

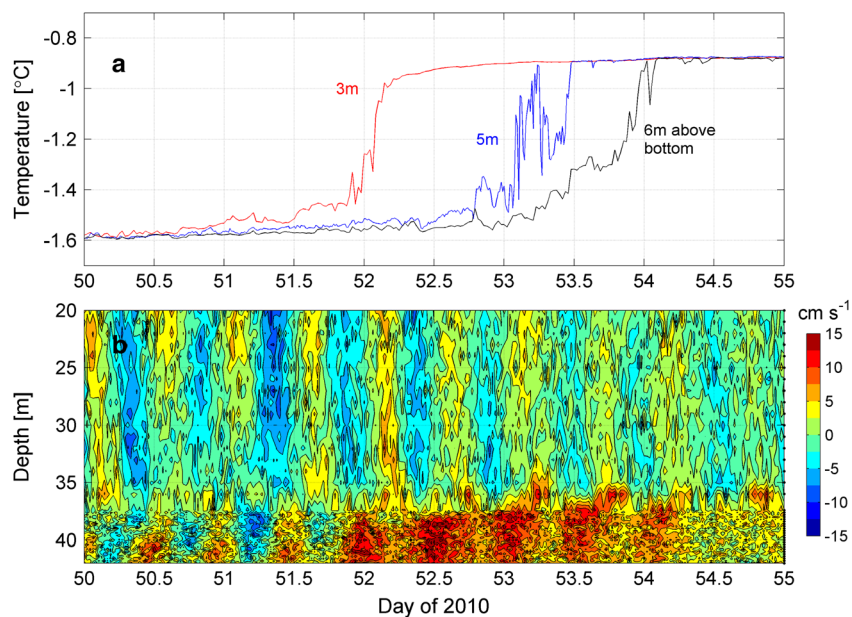


**Figure 5.** (a) Mooring KH temperature [ $^{\circ}\text{C}$ ] from 19 to 24 Feb 2010 from three sensors moored at 3 m (red), 5 m (blue), and 6 m (black) above the sea floor. (b) velocity [ $\text{cm s}^{-1}$ ] along the principal axis ( $160^{\circ}$ ) from 20 to 42 m for 19–24 Feb 2010.

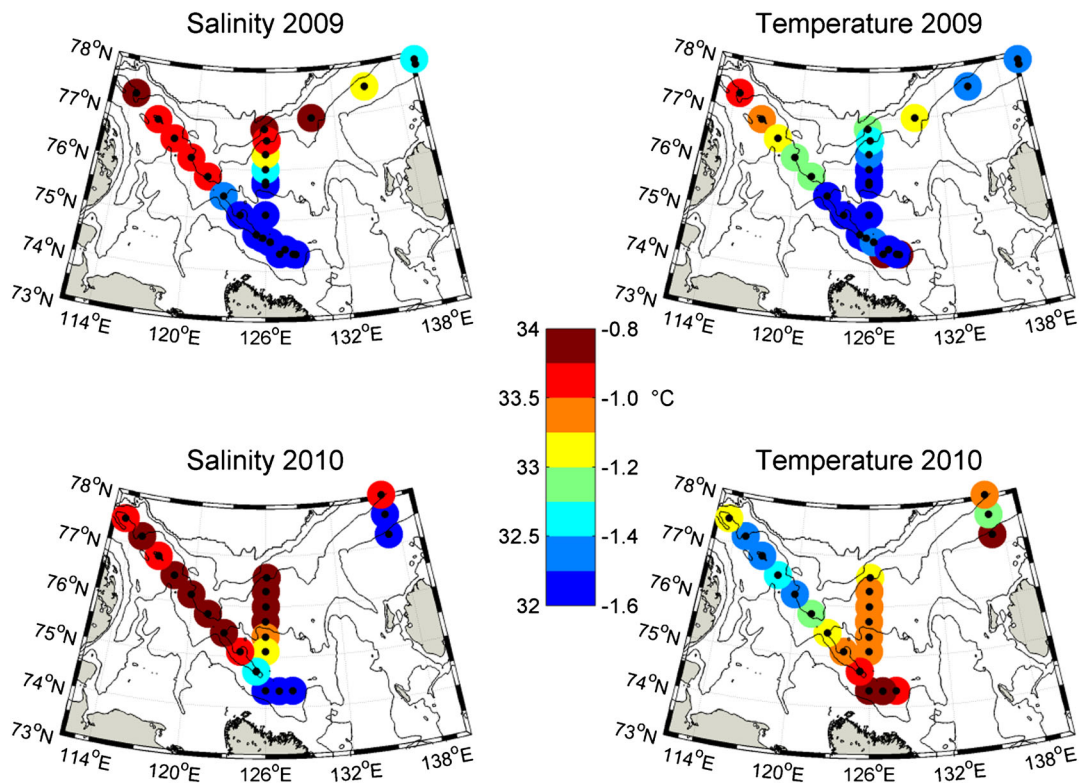


**Figure 6.** Mean lower layer (>25 m) salinity (left) and temperature [ $^{\circ}\text{C}$ ] (right) from the 2009 (top) and 2010 (bottom) CTD surveys. Black dots show exact station locations.

the northwestern CTD transect (Figure 6) from  $-1.6$  to  $-0.9^{\circ}\text{C}$  ( $32.5$  to  $>33.5$ ) toward the shelf break in 2009. Although we lack further observation from the shelf break, it is reasonable to assume that the warm and saline waters were upwelled from the continental slope, based on previous transects across the northwestern Laptev Sea slope, which showed the corresponding temperature and salinity values at a depth between 50 and 100 m [Schauer *et al.*, 1997]. Furthermore, modeling results by Yang [2006] showed maximum wind-driven upwelling rates over the northwestern Laptev Sea slope, which strengthens our assumption on the origin of this water mass and implies that this region may be of particular interest for shelf-basin exchange processes.

[21] In order to investigate the frequency of occurrence of thermohaline properties similar to those measured in winter 2010, we screened historical CTD profiles from the Laptev Sea shelf (see data and methods section for data description) for temperature and salinity of  $>-1.0^{\circ}\text{C}$  and  $>33$  and found these characteristics in only  $\sim 1\%$  of the profiles at depths between 30 and 60 m (30 m: 10 out of 819 profiles; 40 m: 4/380; 50 m: 1/151; 60 m: 0/62). All of these occurrences were from profiles measured between July and October, which suggests that equally warm and saline waters can occur but are not frequent on the shallow (30–60 m) Laptev Sea shelf. Waters with the above characteristics were not previously measured there in winter, which underlines the necessity of using moored systems to generate year-round datasets in under-sampled regions such as the Siberian shelves.

[22] The warm and saline waters apparently continued to spread across the inner- and central shelves. Nearly 100 days after arriving at KH, our second mooring at a water depth of 33 m (AN) ( $\sim 100$  km away from KH, Figure 1), registered a

strong increase in temperature and salinity. The increase at AN coincided with southward currents and was unrelated to the February 2010 KH inflow event, which implies a larger-scale, shelfwide influence of the warm and saline waters as indicated by the September 2010 CTD survey (Figure 6). Similar to conditions at KH in fall 2009, AN was characterized by strong density (i.e., temperature and salinity) variability during the mobile ice period before remaining constant from February until June 2010, when AN recorded a water mass with properties (temperature  $-1.2^{\circ}\text{C}$ , salinity  $\sim 33$ ), nearly similar to those measured at KH (Figures 3a and 3b). In late summer, the near-bottom CTD at AN registered the downward mixing of the summer-warmed and -freshened upper layer, measured as a temperature (salinity) increase (decrease). The mooring records and the 2009 and 2010 CTD surveys suggest that warm and saline waters with a northwestern shelf origin propagated south- and eastward and likely occupied a significant portion of the inner and central Laptev Sea shelves. Our moorings suggest that the anomalies persisted until the mooring recovery in September 2010, at least in those regions deep enough (KH) for stratification to shield the bottom waters from late summer storms.

### 3.4. Upwelling-favorable Winds, Ice Drift, and Bottom-intensified Currents

[23] The near-bottom inflow events introduced the hydrographic changes to the inner Laptev Sea mooring site KH and dominated the flow structure during the late winter solid pack ice period. A visual examination of pressure anomalies, ice drift, winds, and bottom currents clearly suggests a relationship between these independent variables, in particular

during the stronger bottom flow events as seen around year-day 86 or 111 (Figure 7). Currents, pressure, and ice drift were low-pass filtered for periods  $>2$  days based on decorrelation time scales for NCEP winds near KH of 2.5 to 3 days. We then subsampled the mooring data to match the 6-hourly NCEP intervals in order to perform correlations. Southeasterly winds showed the highest correlations with 30 h lagged sea level ( $R^2=0.45$ ,  $p < 0.01$ ) and 6 hourly lagged northward ice drift ( $R^2=0.49$ ,  $p < 0.01$ ). Ice drift and sea level are most correlated with a 6 h lag ( $R^2=0.40$ ,  $p < 0.01$ ). Generally, southeasterly (negative) winds coincide with negative pressure anomalies, north-northwestward (positive implying offshore) ice drift, and southeastward (positive implying onshore) near-bottom flow (Figure 7). The direction of near-bottom currents (onshore versus offshore) corresponds to sea level anomalies, in early as well as in late winter. Between November 2009 and January 2010, both positive and negative pressure anomalies occurred, with predominant westerly winds and westward near-bottom currents. However, westward bottom currents are rarely seen later in winter, despite occasional onshore winds. Positive pressure anomalies in late winter are equally rare, which is due to the presence of immobile landfast ice shoreward of KH, inhibiting onshore ice drift as described above. Similar conditions were seen in a yearlong bottom pressure record near the fast ice edge in the eastern Laptev Sea ( $75.2^\circ\text{N}$ ,  $130.8^\circ\text{E}$ ) in 1999. Then, sea level anomalies were also exclusively negative during February–April (not shown), likely due to the presence of landfast ice, and some intrusions of denser water were observed following offshore winds [Dmitrenko *et al.*, 2010].

[24] The Laptev Sea coastline resembles the shape of a large bay as opposed to comparatively straight narrow shelves such as the Beaufort shelf, and the along- and cross-shore directions are not immediately obvious, which is in addition complicated by a landfast ice edge that varies through the course of the winter (Figure 2). Further underlined by the maximum correlations between southeasterly winds and the principal axis ( $160^\circ$ ) of the bottom-intensified currents,

we loosely employ the terms “alongshore” and “upwelling-favorable” for winds toward the northwest, and north-south for the “cross-shore” direction. Note that we use “upwelling-favorable” to describe those winds leading to bottom onshore transport. In the presence of a slope, bottom onshore transport can lead to upward motion, but due to limited data, we will not discuss the fate of water parcels inshore of KH. With the following calculations, we compare the ADCP-measured bottom transport with a theoretical surface Ekman transport computed from the ice drift component  $30^\circ$  to the left of the principal axis of the bottom currents. The orientation of wind, ice, and currents are suggested by our data and outlined in Figure 8.

[25] For simplicity, we consider a two-dimensional setup of a two-layer water column (Figure 8). We assume long time scales (time  $> f^{-1}$ ) and no variation in alongshore sea level, so that the cross-shelf momentum equation (not shown) reduces to the Ekman balance:

$$U_{\text{surf}} = \tau_s^y \rho_0^{-1} f^{-1}, \quad (2)$$

where the surface Ekman transport  $U_{\text{surf}}$  is dependent on the surface stress  $\tau_s^y$ , the density  $\rho$ , and Coriolis force  $f$ . In the presence of sea ice,  $\tau_s^y$  is dependent on the ice drift velocity  $v_{\text{ice}}$ , inferred from the ADCP’s bottom track, as well as on the frictional coupling coefficient  $r$ :

$$\tau_s^y = \rho r v_{\text{ice}} \quad (3)$$

[26] We computed variable  $r$  between  $10^{-4}$  and  $10^{-3}$ , dependent on the daily standard deviation of bottom track depth, implying that a higher standard deviation mimics a higher degree of roughness on the underside of the ice, increasing the frictional coupling between ice and ocean [Lu *et al.*, 2011].

[27] Since the total cross-shelf transport in a two-dimensional setup is zero [Dever, 1997], the surface Ekman transport is balanced by the bottom transport, which we calculated from the integrated cross-shelf ADCP velocities from the sea floor

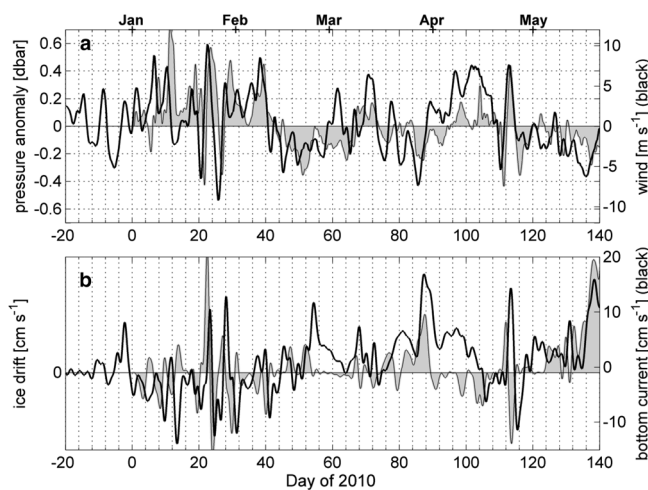


**Figure 7.** (a) CTD measured near-bottom pressure anomalies (gray) and NCEP winds (black; positive values indicate winds to the southeast). (b) Meridional ice drift velocity [ $\text{cm s}^{-1}$ ] derived from the ADCP in bottom track mode (gray, positive values indicate northward drift) and near-bottom currents along the principal axis ( $160^\circ$ ) [ $\text{cm s}^{-1}$ ] (black; positive values indicate flow to the southeast) versus day of year 2010. The first day of each month is marked at the top of Figure 7a.

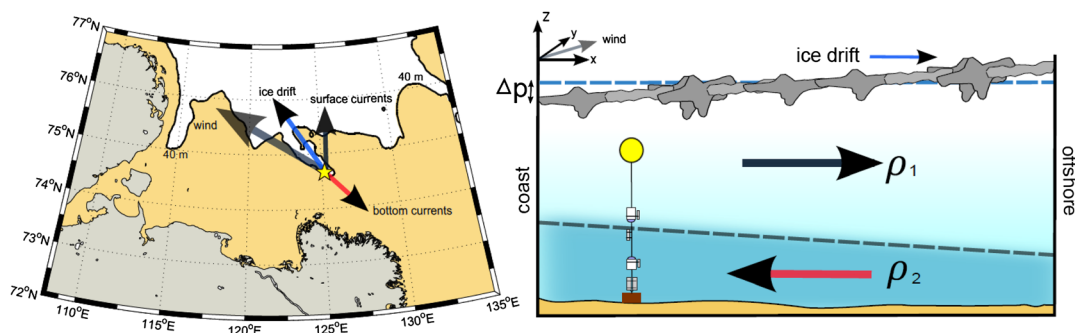


**Figure 8.** (Left) Schematic overview of the affect of upwelling-favorable winds. Arrows (not to scale) indicate the general direction of winds, ice drift, and surface and bottom currents during bottom-intensified flow events at the KH mooring location (yellow star) as highlighted in the text. The shading indicates water depth  $< 40$  m in order to accentuate the bathymetry. (Right) Schematic showing a two-layer water column under the influence of upwelling-favorable winds in the cross-shore direction with the coast on the left and the outer shelf on the right in a two-dimensional setup. Ice drift follows the general wind direction and negative pressure anomalies ( $\Delta P$ ) measured by the SBE37, implying a sea level reduction due to offshore winds, compensated by onshore flow in the bottom layer.

to the depth  $d$  at the base of the pycnocline, as inferred from the velocity shear (Figure 3):

$$U_{\text{bot}} = \int_0^d u dz \quad (4)$$

[28] The surface and bottom transports estimated by (2) and (4) overall compare favorably in direction, although they lack exact quantitative agreement (Figure 9). Discrepancies can be expected for a multitude of reasons, such as strong uncertainties in ice-ocean coupling, the role of ice keels, changes in stratification between early and late winter, or the role of coastline and fast ice edge as explained above. In addition, topographic steering likely occurs, so that we may expect a response in bottom currents even if wind directions deviate from strictly “upwelling-favorable”. Overall, and to first order, the observed onshore bottom-intensified currents occur as a response to wind- and ice-driven surface

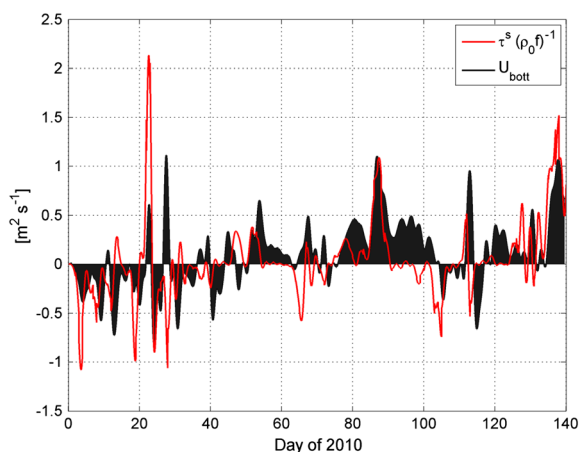


**Figure 9.** Surface Ekman transport (red) and near-bottom transport (black) [ $\text{m}^2 \text{s}^{-1}$ ] versus day of the year in 2010 at mooring KH. The surface transport is based on observed ice drift velocities, and bottom transport is based on integrated ADCP-measured velocities below the lower pycnocline.

transport. Similar two-dimensional circulation patterns were observed on the Beaufort Sea shelf, where moorings recorded shoreward transport following offshore (i.e., upwelling-favorable) winds [Schulze and Pickart, 2012]. They observed this process in all seasons, although most prominently under a partial ice cover when stress is transferred from ice to ocean most effectively.

[29] Two previous mooring deployments at the KH location did not show any considerable bottom-intensified currents, and we expect that the stratification induced by the  $> 2 \text{ kg m}^{-3}$  density increase (corresponding to a buoyancy frequency of  $N \sim 0.06 \text{ s}^{-1}$ ) event in February 2010 is a key for these observations. Harms *et al.* [2003] discussed salt intrusions in the Kara Sea, which occur often in the Yenisey estuary but rarely in the Ob estuary. Their modeling study suggested that these differences arise from the specific alignment of the estuary along the principal axis of the winds leading to strong offshore surface transport of freshwater, which is compensated for by the intrusion of saline bottom water. Furthermore, the strong stratification prevalent at the Yenisey estuary appeared to be a necessary precondition. This agrees with observations from a shallow midlatitude shelf, where upwelling-favorable winds lead to vigorous onshore transport near the bottom during periods of enhanced stratification, while the cross-shelf circulation under the same wind forcing halted as soon as stratification was eroded [Lentz, 2001]. Lentz’s [2001] and Harms *et al.*’s [2003] emphasis on stratification likely applies to our observations, which underlines the need to resolve the structure of the water column during future experiments in the Laptev Sea.

[30] Similar inflow events were absent at the  $\sim 100$  km distant AN mooring site during winter. The magnitude squared coherence between pressure anomalies from moorings KH and AN is  $> 0.9$  for periods  $> 2$  days, which implies a larger-scale impact of winds and ice drift on sea level oscillations; however, no enhanced near-bottom under-ice currents were recorded at AN in mid-winter. Currents at AN were generally weak ( $\sim 5 \text{ cm s}^{-1}$ ) and if stronger ( $\sim 10 \text{ cm s}^{-1}$ ), barotropic. Wind-driven currents of magnitude  $> 20 \text{ cm s}^{-1}$  occurred in late May at the onset of the open water season and finally advected saline ( $\sim 33$ ) and warmer ( $> -1.2^\circ\text{C}$ ) waters to AN,

nearly similar to those that arrived at KH in February. Again, the missing response to upwelling-favorable winds at AN could be explained by a suite of environmental differences related to water depth, topography or perhaps most importantly the lack of stratification [Lentz, 2001]. Furthermore, AN is located near the fast ice edge (Figure 1), where ice edge dynamics [Kasper and Weingartner, 2012] may dominate over other processes and hence dilute the clear ocean response to winds and ice drift observed at KH.

#### 4. Summary

[31] ADCP, near-bottom CTD, and ADCP-derived ice drift data from two year-round oceanographic moorings on the inner Laptev Sea shelf complemented by shelfwide CTD surveys in 2009 and 2010 were used to highlight a recent increase in near-bottom temperature and salinity in the Laptev Sea (Figure 3), first observed in September 2009 on the northwestern shelf (Figure 6). In particular, we identified wind-driven (upwelling-favorable) ice drift and Ekman transport as the key mechanisms that forced the shoreward propagation of the anomalies in the form of a series of bottom-intensified flow events observed under the late winter pack ice cover.

[32] Our record revealed three periods distinguishable by sea ice cover, currents, and shear structure (Figure 3): (1) November to January: thin, mobile ice cover; (2) February to mid-May: thick, less mobile ice cover; (3) late May to September: open water season. Our mooring records provided valuable new oceanographic information in particular from the early and late winter seasons. The early winter (period 1) was characterized by enhanced but variable ice drift, contributing to a well-mixed water column by late January, based on strong temperature variability and the steady salinity decrease due to downward mixing of fresher surface waters. The late winter (period 2) showed a series of enhanced near-bottom flow events, the first of which introduced a sudden increase in near-bottom temperature ( $-1.6^{\circ}\text{C}$  to  $-0.9^{\circ}\text{C}$ ) and salinity (29.5 to 33) (Figure 3). Based on velocity shear, the inflowing plume with a density of  $\sim 2 \text{ kg m}^{-3}$  higher than the ambient waters extended 6–10 m above the bottom (Figure 3). A comparison with historical Laptev Sea CTD data showed that the mooring-recorded temperature and salinity values from February 2010 were on rare occasions measured in summer but not previously on the inner shelf in winter. The open water season (period 3) was dominated by surface-intensified wind-driven currents and no longer showed the enhanced bottom flow characteristic for the late winter 2010. Besides the near-bottom pycnocline, a seasonal pycnocline was established at 15 m, and bottom water mass characteristics were preserved until at least the end of the mooring deployment in September 2010 (Figure 4).

[33] The main focus of this paper is on the ice-covered late winter period, which featured the bottom-intensified flow events and the changes in water mass characteristics to warm and saline. A September 2009 CTD survey found these characteristics in bottom waters of the northwestern Laptev Sea shelf from where they spread east- and shoreward across the shelf within the course of 1 year (Figure 6). Our inner-shelf mooring KH recorded episodic onshore flow events which clearly helped to move these warm and saline waters to the inner shelf. Each of these events coincided with

negative pressure anomalies at the mooring during offshore-directed winds and ice drift, implying that they were the barotropic near-bottom response to surface Ekman transport (Figures 7 and 8). A comparison between observed bottom transport and ice drift-derived Ekman transport shows a near-balance between the two (Figure 9), which suggests that, to first order, a simplified two-dimensional description of this process is appropriate. Consistent with previous studies [Lentz, 2001; Harms *et al.*, 2003], we assume that the strong stratification induced by the warm and saline water was a necessary factor in the generation of the onshore flow events. Despite variable wind directions in late winter, pressure anomalies at the mooring were only negative, which implies that the presence of landfast ice  $\sim 50$ – $70$  km south of the mooring blocks an Ekman response to downwelling-favorable winds, suggesting that, at this location, the wind-driven bottom cross-shore transport is a one-way (onshore) winter process only.

#### 5. Discussion and Implications

[34] Despite the large portion of the Arctic composed of Siberian shelves, comprehensive year-round oceanographic data there are rare. Our observations present for the first time evidence of bottom-intensified under-ice currents in response to upwelling-favorable winds transporting anomalously warm and saline waters to the inner shelf. The observations highlight a wind-driven under-ice circulation that clearly differs from the surface-intensified circulation during the open water season. The winter 2010 inflow carried a significant amount of salt and heat to the inner shelf, with possible implications for sea ice and biota. CTD measurements from September 2009 showed equally high temperatures and salinities on the northwestern shelf, but processes and conditions in this region are not well understood due to difficult access and a lack of data. While these temperature and salinity characteristics point to a basin origin [Schauer *et al.*, 1997], solar heating of shelf waters may also become more important during extended open water seasons as discussed by Hölemann *et al.* [2011] for Laptev Sea conditions during the anomalously low sea ice extent in 2007 [Stroeve *et al.*, 2008]. While both advection and solar radiation play a role for the heat budget on the Laptev Sea shelf, the relative importance of each is not yet clear and will be an important question to answer in future studies, especially with respect to a changing climate and expected prolongations of the open water season [Stroeve *et al.*, 2007].

[35] Above-freezing temperatures can be maintained in bottom waters throughout the fall cooling and mixing period due to freshwater stratification and, if released toward the surface, can lead to delays in freezeup or impact a winter-time ice cover. This depends on the strength of stratification, which on the inner Laptev Sea shelf depends on the distribution of the Lena freshwater governed by large-scale atmospheric summer conditions [Shpaikher *et al.*, 1972; Proshutinsky and Johnson, 1997; Steele and Ermold, 2004] as well as on the strength of under-ice mixing. However, despite its importance, only a few studies are currently available on under-ice mixing on Siberian shelves [Lenn *et al.*, 2011; Dmitrenko *et al.*, 2012]. On the Chukchi Sea shelf, for instance, under-ice mixing was found to be small [Rainville and Woodgate, 2009]. Semidiurnal tides in most Laptev Sea shelf regions, however, far exceed those on the Beaufort and Chukchi shelves

[Kowalik and Proshutinsky, 1994; Padman and Erofeeva, 2004] and provide kinetic energy whose contribution to mixing is not yet understood. For instance, whether or not the dimensions of the February 2010 inflow favor entrainment and mixing with background waters is estimated through the internal Froude number  $F$ , as the inverse of the gradient Richardson number  $Ri = (g'h)/\Delta u^2$ .  $Ri$  is based on the reduced gravity  $g' = g(\rho_s - \rho_i)/\rho_i$ , the plume thickness  $h$ , and the velocity difference  $\Delta u$  across the interface [Weingartner et al., 1998]. With background shelf and plume densities of  $\rho_s = 1024 \text{ kg m}^{-3}$  and  $\rho_i = 1026 \text{ kg m}^{-3}$ , respectively, a plume thickness of 5–10 m,  $\Delta u = 0.1\text{--}0.2 \text{ m s}^{-1}$ , and  $g = 9.81 \text{ m s}^{-2}$ ,  $Ri \gg 1$ , so that  $F \ll 1$ , which means that the flow is subcritical and entrainment negligible. However, the maximum shear depth (Figure 3c) decreases and indicates upward propagation of the density interface and hence lower layer vertical mixing after the first inflow event. Indeed, spectral analysis of upper (10–20 m) and lower (30–40 m) layer currents during February–April 2010 (Figure 10) shows that the bottom inflow events enhanced the energy at semidiurnal frequency in the lower layer and exceeded the upper layer energy by 60%. The inertial (0.0806 cph) and the  $M_2$ -tidal (0.0805 cph) frequencies at KH (74.7°N) are nearly identical and hence inseparable, and we expect that the high semidiurnal energy in the lower layer is due to near-inertial waves and/or baroclinic tides amplified at the plume's upper interface. Lenn et al. [2011] showed that tidal mixing on the outer Laptev Sea shelf occurs intermittently, and we expect that the same holds true at our mooring location, where peak shear levels generally occur during spring tides (not shown). Our observations suggest that these bottom-intensified currents support low-frequency cross-shelf transport and in addition increase the kinetic energy at semidiurnal frequency and hence likely support under-ice mixing. Laptev Sea bottom waters sometimes show elevated nutrient levels in an otherwise nutrient-poor system [Nitishinsky et al., 2007], which underlines the need to quantify vertical under-ice mixing in order to understand the vertical distribution of energy and biogeochemical properties on this shelf.

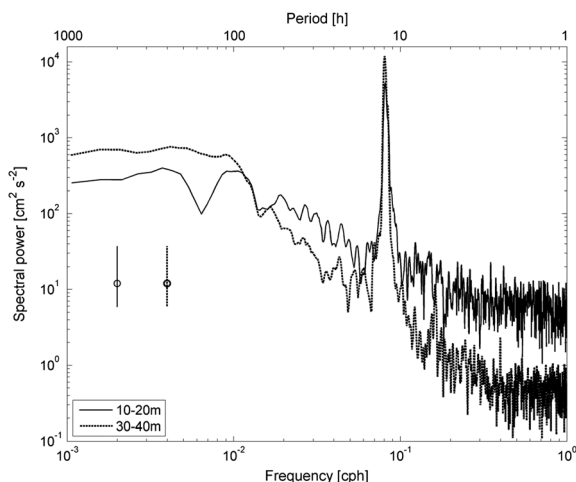


**Figure 10.** Spectral power [ $\text{cm}^2 \text{s}^{-2}$ ] of ADCP velocities from 20 February to 10 May 2010 versus frequency [cph]. The spectra show a comparison between upper (averaged over 10–20 m, solid) and lower layer (30–40 m, dashed) major axis currents. Vertical bars show the 95% confidence intervals.

[36] In early winter 2009/2010 during enhanced polynya activity at the fast ice edge and ice motion at our mooring site, we observed a freshening of the bottom waters as a consequence of vertical freshwater redistribution, likely as a consequence of the combined mixing effects induced by tides at the pycnocline and bottom boundary layer [Lenn et al., 2011] and by ice-ocean stress near the surface [Kowalik and Proshutinsky, 1994; Skillingstad et al., 2003]. Even though Laptev Sea mooring data are limited, a near-bottom density decrease due to downward mixing of fresher surface waters during nearby polynya activity has been observed before [Hölemann et al., 2011], and we expect that this process is not entirely unusual for freshwater-influenced Arctic inner-shelf regions. While we lack mid-winter profiles from the outer shelf, it appears likely that regions with a higher mean salinity away from the Lena freshwater source maintain denser bottom waters and that horizontal density gradients should exist from the mooring location toward the shelf break. This would induce motion and implies that gravity currents should exist that flow into those polynya regions with “less-dense bottom water formation” as opposed to commonly accepted dense water formation regions on Arctic shelves with resulting gravity currents away from the polynya [Chapman and Gawarkiewicz, 1997; Chapman, 1999; Backhaus et al., 1997; Weingartner et al., 1998; Williams et al., 2007]. The relative importance of this process is perhaps secondary, and quantification requires a different set of observations or process modeling studies which is beyond the scope of this paper. In aggregate, our results suggest that the shelf's under-ice flow regime is intimately coupled to winds, ice drift, and stratification. Winds govern the ice drift [Eicken et al., 1997] and drive oceanic currents through both surface friction and barotropic response flows to Ekman surface transport. Our 2010 data revealed the unequal affect of landfast ice on up- and downwelling-favorable winds, and while we currently lack a comprehensive understanding of the under-ice circulation on the Laptev Sea shelf, it appears inevitable that changes in thickness, duration, extent, and in particular mobility of the seasonal ice cover will change the winter circulation on this shelf.

[37] **Acknowledgments.** Financial support for the “Laptev Sea Systems” project was provided by the German Federal Ministry of Education and Research (grant BMBF 03G0639A) and the Ministry of Education and Science of the Russian Federation. NCEP reanalysis data were provided by the NOAA-CIRES Climate Diagnostics Center, Boulder, CO, USA, from their Web site at <http://www.cdc.noaa.gov/>. Satellite-based ice motion information was provided by CERSAT/IFREMER. ENVISAT SAR images were obtained through ESA AO-project 9429, “The use of ENVISAT ASAR imagery for generation and validation of Arctic and Antarctic landfast sea ice masks.” We thank the captains and crew of the RV *Yakov Smirnitky* and RV *Nikolay Evgenov*, as well as project members for support during the Transdrift XVI and XVII cruises. A. Novikhin led the CTD data collection effort during the expeditions. We acknowledge T. Klagge for his invaluable effort during the mooring deployment and recovery and H. Kassens and L. Timokhov for their energy and skills in managing the project. We greatly appreciate discussions and comments from U. Schauer and B. Rabe. We thank the editor and three reviewers for helpful comments, which significantly improved the manuscript.

## References

- Aagaard, K., L. K. Coachman, and E. C. Carmack (1981), On the halocline of the Arctic Ocean, *Deep Sea Res.*, 28, 529–545.  
 Aagaard, K. (1989), A synthesis of the Arctic Ocean circulation, *Rapp. P.-v. Réun. Cons. Int. Explor. Mer*, 188, 11–22.  
 Alexandrov, V. Y., T. Martin, J. Kolatschek, H. Eicken, M. Kreyscher, and A. P. Makshtas (2000), Sea ice circulation in the Laptev Sea and ice

- export to the Arctic Ocean: Results from satellite remote sensing and numerical modeling, *J. Geophys. Res.*, *105*(C7), 17143–17159.
- Backhaus, J. A., H. Fohrmann, J. Kaempf, and A. Rubino (1997), Formation and export of water masses produced in Arctic shelf polynyas—Process studies of oceanic convection, *J. Mar. Sci.*, *54*, 366–382.
- Bareiss, J., and K. Gørgen (2005), Spatial and temporal variability of sea ice in the Laptev Sea: Analyses and review of satellite passive-microwave data and model results, 1979 to 2002, *Glob. Planet. Change*, *48*(1–3), 28–54.
- Bauch, D., I. A. Dmitrenko, S. A. Kirillov, C. Wegner, J. Hölemann, S. Pivovarov, L. A. Timokhov, and H. Kassens (2009), Eurasian Arctic shelf hydrography: Exchange and residence time of southern Laptev Sea waters, *Cont. Shelf Res.*, *29*, 1815–1820, doi:10.1016/j.csr.2009.06.1009.
- Chapman, D. C., and G. Gawarkiewicz (1997), Shallow convection and buoyancy equilibration in an idealized coastal polynya, *J. Phys. Oceanogr.*, *27*, 555–566.
- Chapman, D. C. (1999), Dense water formation beneath a time-dependent coastal polynya, *J. Phys. Oceanogr.*, *29*, 807–820.
- Dethleff, D., P. Loewe, and E. Kleine (1998), The Laptev Sea flow lead—Detailed investigation on ice formation and export during 1991/92 winter season, *Cold Reg. Sci. Technol.*, *27*, 3, pp. 225–243.
- Dethleff, D. (2010), Dense water formation in the Laptev Sea flow lead, *J. Geophys. Res.*, *115*, C12022, doi:10.1029/2009JC006080.
- Dever, E. P. (1997), Wind-forced cross-shelf circulation on the northern California shelf, *J. Phys. Oceanogr.*, *27*, 1566–1580.
- Dmitrenko, I. A., K. N. Tyshko, S. A. Kirillov, H. Eicken, J. A. Hölemann, and H. Kassens (2005), Impact of flow polynyas on the hydrography of the Laptev Sea, *Glob. Planet. Change*, *48*, 9–27, doi:10.1016/j.gloplacha.2004.12.016.
- Dmitrenko, I. A., S. A. Kirillov, and L. B. Tremblay (2008), The longterm and interannual variability of summer fresh water storage over the eastern Siberian shelf: Implication for climatic change, *J. Geophys. Res.*, *113*, C03007, doi:10.1029/2007JC004304.
- Dmitrenko, I. A., S. A. Kirillov, L. B. Tremblay, D. Bauch, J. A. Hölemann, T. Krumpen, H. Kassens, C. Wegner, G. Heinemann, and D. Schröder (2010), Impact of the Arctic Ocean Atlantic water layer on Siberian shelf hydrography, *J. Geophys. Res.*, *115*, C08010, doi:10.1029/2009JC006020.
- Dmitrenko, I. A., S. A. Kirillov, E. Bloskhina, and Y.-D. Lenn (2012), Tide-induced vertical mixing in the Laptev Sea coastal polynya, *J. Geophys. Res.*, *117*, C00G14, doi:10.1029/2011JC006966.
- Eicken, H., E. Reimnitz, V. Alexandrov, T. Martin, H. Kassens, and T. Viehoff (1997), Sea-ice processes in the Laptev Sea and their importance for sediment export, *Cont. Shelf Res.*, *17*(2), 205–233.
- Ernsdorf, T., D. Schröder, S. Adams, G. Heinemann, R. Timmermann, and S. Danilov (2011), Impact of atmospheric forcing data on simulations of the Laptev Sea polynya dynamics using the sea-ice ocean model FESOM, *J. Geophys. Res.*, *116*, C12038, doi:10.1029/2010JC006725.
- Ezraty, R., F. Girard-Ardhuin, and D. Croiz-Fillon (2010), Sea ice drift in the central Arctic using the 89 GHz brightness temperatures of the Advanced Microwave Scanning Radiometer, <http://www.ifremer.fr/cersat.1317>.
- Guay, C. K., R. D. Falkner, R. D. Muench, M. Mensch, M. Frank, and R. Bayer (2001), Wind-driven transport pathways for Eurasian Arctic river discharge, *J. Geophys. Res.*, *106*, 11,469–11,480.
- Harms, I. H., U. Hübner, J. O. Backhaus, M. Kulakov, V. Stanovoy, O. V. Stepanets, L. A. Kodina, and R. Schlitzer (2003), Salt intrusions in Siberian river estuaries: Observations and model experiments in Ob and Yenisei, in *Siberian River Run-off in the Kara Sea: Characterisation, Quantification, Variability, and Environmental Significance*, Proc. Mar. Sci., vol. 6, edited by R. Stein et al., pp. 27–45, Elsevier, New York.
- Hölemann, J. A., S. Kirillov, T. Klage, A. Novikhin, H. Kassens, and L. Timokhov (2011), Near-bottom water warming in the Laptev Sea in response to atmospheric and sea ice conditions in 2007, *Polar Res.*, *30*, 6425, doi:10.3402/polar.v30i0.6425.
- Howard, S. L., J. Hyatt, and L. Padman (2004), Mixing in the pycnocline over the western Antarctic Peninsula Shelf during Southern Ocean GLOBEC, *Deep Sea Res., Pt. II*, *51*, 1965–1979, doi:10.1016/j.dsr2.2004.08.002.
- Hyatt, J., M. Visbeck, R. C. Beardsley, and W. Brechner Owens (2008), Estimating sea ice coverage, draft, and velocity in Marguerite Bay (Antarctica) using a subsurface moored upward-looking acoustic Doppler current profiler (ADCP), *Deep Sea Res., Pt. II*, *55*, 351–364.
- Ivanov, V. V., and P. N. Golovin (2007), Observations and modeling of dense water cascading from the northwestern Laptev Sea shelf, *J. Geophys. Res.*, *112*, C09003, doi:10.1029/2006JC003882.
- Jackson, J. M., E. C. Carmack, F. A. McLaughlin, S. E. Allen, and R. G. Ingram (2010), Identification, characterization and change of the near surface temperature maximum in the Canada Basin, 1993–2008, *J. Geophys. Res.*, *115*, C05021, doi:10.1029/2009JC005265.
- Jakobsson, M., R. Macnab, L. Mayer, R. Anderson, M. Edwards, J. Hatzky, H. W. Schenke, and P. Johnson (2008), An improved bathymetric portrayal of the Arctic Ocean: Implications for ocean modeling and geological, geophysical and oceanographic analyses, *Geophys. Res. Lett.*, doi:10.1029/2008gl033520.
- Kasper, J. L., and T. J. Weingartner (2012), Modeling winter circulation under landfast ice: The interaction of winds with landfast ice, *J. Geophys. Res.*, *117*, C04006, doi:10.1029/2011JC007649.
- Kowalik, Z., and A. Y. Proshutinsky (1994), The Arctic Ocean tides, in *The Polar Oceans and Their Role in Shaping the Global Environment*, Geophys. Monogr. Ser., vol. 85, edited by O. M. Johannessen, R. D. Muench, and J. E. Overland, pp. 137–158, AGU, Washington, D. C.
- Krumpen, T., et al. (2011), Sea ice production and water mass modification in the eastern Laptev Sea, *J. Geophys. Res.*, *116*, C05014, doi:10.1029/2010JC006545.
- Lenn, Y. D., P. J. Wiles, S. Torres-Valdes, E. P. Abrahamsen, T. P. Rippeth, J. H. Simpson, S. Bacon, S. W. Laxon, I. Polyakov, V. Ivanov, and S. Kirillov (2009), Vertical mixing at intermediate depths in the Arctic boundary current, *Geophys. Res. Lett.*, *36*, L05061, doi:10.1029/2008GL036792.
- Lenn, Y.-D., T. P. Rippeth, C. P. Old, S. Bacon, I. Polyakov, V. Ivanov, and J. Hölemann (2011), Intermittent intense turbulent mixing under ice in the Laptev Sea continental shelf, *J. Phys. Oceanogr.*, *41*, 531–547, doi:10.1175/2010JPO4425.1.
- Lentz, S. J. (2001), The influence of stratification on the wind-driven cross-shelf circulation over the North Carolina shelf, *J. Phys. Oceanogr.*, *31*(9), 2749–2760.
- Lu, P., Z. Li, B. Cheng, and M. Leppäranta (2011), A parameterization of the ice-ocean drag coefficient, *J. Geophys. Res.*, *116*, C07019, doi:10.1029/2010JC006878.
- Martin, S., and P. Kauffman (1981), A field and laboratory study of wave dumping by grease ice, *J. Glaciol.*, *27*, 96, 283–313.
- Martin, S., and D. J. Cavalieri (1989), Contributions of the Siberian Shelf polynyas to the Arctic Ocean intermediate and deep water, *J. Geophys. Res.*, *94*(C9), 12,725–12,738, doi:10.1029/JC094iC09p12725.
- Nitishinsky, M., L. G. Anderson, and J. A. Hölemann (2007), Inorganic carbon and nutrient fluxes on the Arctic Shelf, *Cont. Shelf Res.*, *27*, 1584–1599.
- Padman, L., and S. Erofeeva (2004), A barotropic inverse tidal model for the Arctic Ocean, *Geophys. Res. Lett.*, *31*, L02303, doi:10.1029/2003GL019003.
- Perovich, D. K., J. A. Richter-Menge, K. F. Jones, and B. Light (2008), Sunlight, water, and ice: Extreme Arctic sea ice melt during the summer of 2007, *Geophys. Res. Lett.*, *35*, L11501, doi:10.1029/2008GL034007.
- Pickart, R. S., G. W. K. Moore, D. J. Torres, P. S. Fratantoni, R. A. Goldsmith, and J. Yang (2009), Upwelling on the continental slope of the Alaskan Beaufort Sea: Storms, ice, and oceanographic response, *J. Geophys. Res.*, *114*, C00A13, doi:10.1029/2008JC005009.
- Polyakov, I. V., A. Pnyushkov, R. Rember, V. V. Ivanov, Y.-D. Lenn, L. Padman, and E. C. Carmack (2012), Mooring-based observations of the double-diffusive staircases over the Laptev Sea slope, *J. Phys. Oceanogr.*, *42*, 95–109, doi:10.1175/2011JPO4606.1.
- Proshutinsky, A. Y., and M. A. Johnson (1997), Two circulation regimes of the wind-driven Arctic Ocean, *J. Geophys. Res.*, *102*, 12,493–12,514.
- Rainville, L., and R. A. Woodgate (2009), Observations of internal wave generation in the seasonally ice-free Arctic, *Geophys. Res. Lett.*, *36*, L23604, doi:10.1029/2009GL041291.
- Rozman, P., J. Hölemann, T. Krumpen, R. Gerdes, C. Köberle, T. Lavergne, S. Adams, and F. Girard-Ardhuin (2011), Validating satellite derived and modelled sea-ice drift in the Laptev Sea with in situ measurements from the winter of 2007/08, *Polar Res.*, *30*, 7218, doi:10.3402/polar.v30i0.7218.
- Rudels, B., H. J. Friedrich, and D. Quadfasel (1999a), The Arctic Circumpolar Boundary Current, *Deep Sea Res., Pt. II*, *46*, 1023–1062, doi:10.1016/S0967-0645(99)00015-6.
- Rudels, B., G. Björk, R. Muench, and U. Schauer (1999b), Double-diffusive layering in the Eurasian Basin of the Arctic Ocean, *J. Mar. Syst.*, *21*, 3–27.
- Rudels, B., R. D. Muench, J. Gunn, U. Schauer, and H. J. Friedrich (2000), Evolution of the Arctic Ocean Boundary current north of the Siberian shelves, *J. Mar. Syst.*, *25*, 77–99.
- Rudels, B. (2012), Arctic Ocean circulation and variability—Advection and external forcing encounter constraints and local processes, *Ocean Sci.*, *8*, 261–286, doi:10.5194/os-8-261-2012.
- Schauer, U., R. D. Muench, B. Rudels, and L. Timokhov (1997), Impact of eastern Arctic shelf waters on the Nansen Basin intermediate layers, *J. Geophys. Res.*, *102*, C2, 2271–3382.
- Schulze, L. M., and R. S. Pickart (2012), Seasonal variation of upwelling in the Alaskan Beaufort Sea: Impact of sea ice cover, *J. Geophys. Res.*, *117*, C06022, doi:10.1029/2012JC007985.

- Shcherbina, A. Y., D. L. Rudnick, and L. D. Talley (2005), Ice-draft profiling from bottom-mounted ADCP, *J. Atmos. Oceanic Technol.*, *22*, 1249–1266.
- Shpaikher, O., Z. P. Fedorova, and Z. S. Yankina (1972), Interannual variability of hydrological regime of the Siberian shelf seas in response to atmospheric processes (in Russian), *Proc. AARI*, *306*, 5–17.
- Skyllingstad, E. D., C. A. Paulson, W. S. Pegau, M. G. McPhee, and T. Stanton (2003), Effects of keels on ice bottom turbulence exchange, *J. Geophys. Res.*, *108*(C12), 3372, doi:10.1029/2002JC001488.
- Steele, M., and W. Ermold (2004), Salinity trends on the Siberian shelves, *Geophys. Res. Lett.*, *31*, L24308, doi:10.1029/2004GL021302.
- Stroeve, J., M. M. Holland, W. Meier, T. Scambos, and M. C. Serreze (2007), Arctic Sea ice decline: Faster than forecast, *Geophys. Res. Lett.*, *34*, doi:10.1029/2007GL029703.
- Stroeve, J., M. C. Serreze, S. Drobot, S. Gearhead, M. M. Holland, J. Maslanik, W. Meier, and T. Scambos (2008), Arctic sea ice plummets in 2007, *EOS* *89*(2):13–14, doi:10.1029/2008EO020001.
- van Haren, H. (2000), Properties of vertical current shear across stratification in the North Sea, *J. Mar. Res.*, *58*(2), 465–491.
- Weingartner, T. J., D. J. Cavalieri, K. Aagaard, and Y. Sasaki (1998), Circulation, dense water formation, and outflow on the northeast Chukchi shelf, *J. Geophys. Res.*, *103*, 7647–7661.
- Williams, W. J., E. C. Carmack, K. Shimada, H. Melling, K. Aagaard, R. W. Macdonald, and R. G. Ingram (2006), Joint effects of wind and ice motion in forcing upwelling in Mackenzie Trough, Beaufort Sea, *Cont. Shelf Res.*, *26*, 2352–2366, 10.1016/j.csr.2006.06.012.
- Williams, W. J., E. C. Carmack, and R. G. Ingram (2007), Physical oceanography of Polynyas, in *Polynyas: Windows to the World*, Elsevier Oceanography Series, vol. 74, edited by W. O. Smith, Jr., D. G. Barber, pp. 55–86, Elsevier, Amsterdam.
- Willmes, S., S. Adams, D. Schroeder, and G. Heinemann (2011), Spatiotemporal variability of polynya dynamics and ice production in the Laptev Sea between the winters of 1979/80 and 2007/08, *Polar Res.*, *30*, 5971, doi:10.3402/polar.v30i0.5971.
- Winsor, P., and G. Björk (2000), Polynya activity in the Arctic Ocean from 1958 to 1997, *J. Geophys. Res.*, *105*(C4), 8789–8803, doi:10.1029/1999JC900305.
- Woodgate, R. A., K. Aagaard, R. D. Muench, J. Gunn, G. Björk, B. Rudels, A. T. Roach and U. Schauer (2001), The Arctic Ocean boundary current along the Eurasian slope and the adjacent Lomonosov Ridge: Water mass properties, transports and transformations from moored instruments, *Deep-Sea Res., Pt. I*, *48*, 8, 1757–1792.
- Yang, J. (2006), The seasonal variability of the Arctic Ocean Ekman Transport and its role in the mixed layer heat and salt fluxes, *J. Climate*, *19*, pp. 5366–5387.
- Zakharov, V. F. (1966), The role of flaw leads off the edge of fast ice in the hydrological and ice regime of the Laptev Sea, *Oceanology*, *6*, 815–821.